

Dimensionality control and rotational symmetry breaking superconductivity in square-planar layered nickelates

Lin Er Chow,¹ Km Rubi,² King Yau Yip,³ Mathieu Pierre,⁴ Maxime Leroux,⁴ Xinyou Liu,³
Zhaoyang Luo,¹ Shengwei Zeng,¹ Changjian Li,⁵ Michel Goiran,⁴ Neil Harrison,² Walter
Escoffier,⁴ Swee Kuan Goh,³ A. Ariando^{1,✉}

*¹Department of Physics, Faculty of Science, National University of Singapore, Singapore
117551, Singapore*

*²National High Magnetic Field Laboratory, Los Alamos National Laboratory, Los Alamos,
New Mexico 87545, USA*

*³Department of Physics, The Chinese University of Hong Kong, Shatin N.T., Hong Kong SAR,
China*

⁴LNCMI, Université de Toulouse, CNRS, INSA, UPS, EMFL, 31400 Toulouse, France

*⁵Department of Materials Science and Engineering, Southern University of Science and
Technology, Shenzhen, 518055, Guangdong, China*

✉To whom correspondence should be addressed: ariando@nus.edu.sg

The interplay between dimensionality and various phases of matter is a central inquiry in condensed matter physics.¹ New phases are often discovered through spontaneously broken symmetry.² Understanding the dimensionality of superconductivity in the high-temperature cuprate analogue – layered nickelates^{3–8} and revealing a new symmetry-breaking state are the keys to deciphering the underlying pairing mechanism. Here, we demonstrate the highly-tunable dimensionality and a broken rotational symmetry state in the superconductivity of square-planar layered nickelates. The superconducting state, probed by superconducting critical current and magnetoresistance within superconducting transition under direction-dependent in-plane magnetic fields, exhibits a C_2 rotational symmetry which breaks the C_4 rotational symmetry of the square-planar lattice. Furthermore, by performing detailed examination of the angular dependent upper critical fields at temperatures down to 0.5 K with high-magnetic pulsed-fields, we observe a crossover from two-dimensional to three-dimensional superconducting states which can be manipulated by the ionic size fluctuations in the rare-earth spacer layer. Such a large degree of controllability is desired for tailoring strongly two/three-dimensional superconductors and navigating various pairing landscapes for a better understanding of the correlation between reduced dimensionality and unconventional pairing. These results illuminate new directions to unravel the high-temperature superconducting pairing mechanism.

Main text

The discovery of high-temperature (high- T_c) superconductivity in the layered cuprates⁹ with quasi-two-dimensional electronic structure and superconductivity prompted the question of the correlation between reduced dimensionality and high-temperature pairing mechanism.¹⁰ Since then, the enthusiasm to unlock the ingredients of high- T_c pairing motivated the discoveries of superconductivity in layered materials such as ruthenates,¹¹ cobaltates,¹² and iron pnictides.¹³ However, none shared the analogue two-dimensional high- T_c cuprate-like pairing mechanism. Standing beside copper in the periodic table, nickel of Ni^{1+} oxidation state in the infinite-layer nickelates RNiO_2 (R = rare-earth) consists of an analogous square-planar NiO_2 layered structure and $3d^9$ electronic structure with lifted orbital degeneracy which resembles the Cu^{2+} state in the high- T_c cuprates. As the ideal cuprate analogue, realising superconductivity in the layered nickelates^{5-8,14} nearly two decades after its theoretical prediction^{3,4} marked an important step in untangling the high- T_c makeup of cuprates.

The reignited excitement in the field propelled further comparison between the newfound layered nickelates and the cuprates.¹⁵⁻²³ One of the most important questions is: whether the superconductivity in nickelates is two-dimensional like the cuprates,^{24,25} or three-dimensional like the high- T_c multiband iron pnictides?²⁶ Answering the question of the dimensionality of superconductivity is the next most critical step in building theoretical models (e.g., interlayer hopping, R-Ni hybridisation, Ni d_{z^2} flat-band)²⁷⁻³¹ to decipher the pairing mechanism and related competing orderings in the strongly-correlated phase diagram.³² The richness of cuprates' phase diagram begs for the discovery of new phases or ordering in the nickelates, which is typically achieved through the identification of spontaneous symmetry-breaking states. For example, a broken translational symmetry state (charge ordering) was reported in the

undoped and underdoped regimes of the hole-doped nickelates.^{33–35} However, a symmetry-breaking state has yet to be observed inside the superconducting dome, except for the broken global gauge symmetry and rotational symmetry in the phase factor of the order parameter, as expected in an unconventional superconductor family.^{21,28} Searching for a symmetry-breaking state inside the superconducting dome is important to the understanding of the interplay between superconductivity and various orderings, especially if quantum critical transition exists in nickelates.

In this article, we investigate the dimensionality of nickelates' superconductivity by performing a detailed analysis of the angular-dependent upper critical fields $H_{c2}(\theta)$ in various hole-doped nickelates at temperatures down to $0.06 T_c$ using high-magnetic pulsed fields. Our results show that neither a purely two-dimensional nor a three-dimensional description is correct. Instead, the dimensionality of layered nickelates is highly tunable and can undergo a crossover from two-dimensional to three-dimensional superconducting states as temperature decreases to the 0 K limit. The dimensionality of superconductivity in the layered nickelates can be manipulated through the ionic size fluctuations in the rare-earth spacer layer with different hole dopants. Therefore, the layered nickelate family is an ideal platform for investigating the relationship between dimensionality and superconducting pairing. In addition, we probe the in-plane anisotropy of the superconductivity by measuring the variation in the superconducting critical current and magnetoresistance within the superconducting transition in a direction-dependent in-plane magnetic field. A C_2 rotational symmetry is observed, which breaks the C_4 rotational symmetry of the lattice structure. Such a rotational symmetry-breaking superconducting state may indicate nematicity in the superconducting phase of the strongly-correlated hole-doped nickelates family.

2D to 3D dimensionality crossover in the superconducting states

Dimensionality of superconductivity in various hole-doped nickelates was investigated by performing polar angular-dependent upper critical fields $H_{c2}(\theta)$ using high pulsed magnetic field up to 55 T with a measurement geometry as shown in **Fig. 1a**. Details of the sample fabrication and characterization techniques are described in the Methods section and presented in the **Extended Data Fig. 1 and Fig. 2**. The $H_{c2}(\theta)$ at the lowest temperatures well below the superconducting transition T_c are shown in **Figs. 1b-c** and **Extended Data Fig. 3**, while the $H_{c2}(\theta)$ at temperatures near the T_c are shown in **Figs. 1d-f**. A cusp-like peak can be observed near $\theta = 90^\circ$ (H_{c2}^{\parallel}) for both Sr-/Ca-doped La-nickelates (**Figs. 1d & f**) and Sr-doped Nd-nickelates (**Fig. 1e**). Such an anisotropic $H_{c2}(\theta)$ is typical for quasi-two-dimensional superconductivity, which can be described by the 2D-Tinkham model:

$$\left[\frac{H_{c2}(\theta) \sin(\theta)}{H_{c2}(90^\circ)} \right]^2 + \left| \frac{H_{c2}(\theta) \cos(\theta)}{H_{c2}(0^\circ)} \right| = 1.$$

All the $H_{c2}(\theta)$ near T_c show a good agreement with the 2D-Tinkham model, as shown by the solid fit curves. The anisotropy ratio $\gamma = H_{c2}^{\parallel}/H_{c2}^{\perp}$ is typically large for a two-dimensional system; for example, $\text{Bi}_2\text{Sr}_2\text{CaCu}_2\text{O}_x$ has a very large $\gamma \sim 150$.²⁴ On the other hand, isotropic 3D-like superconductor such as $(\text{Ba,K})\text{Fe}_2\text{As}_2$ has a small $\gamma \approx 2$ near T_c and $\gamma \approx 1$ at the lowest temperatures.²⁶ The behaviour of nickelates, described by the strongly temperature dependent γ in **Extended Data Fig. 4**, is dissimilar to both the two-dimensional cuprates and isotropic iron pnictides.

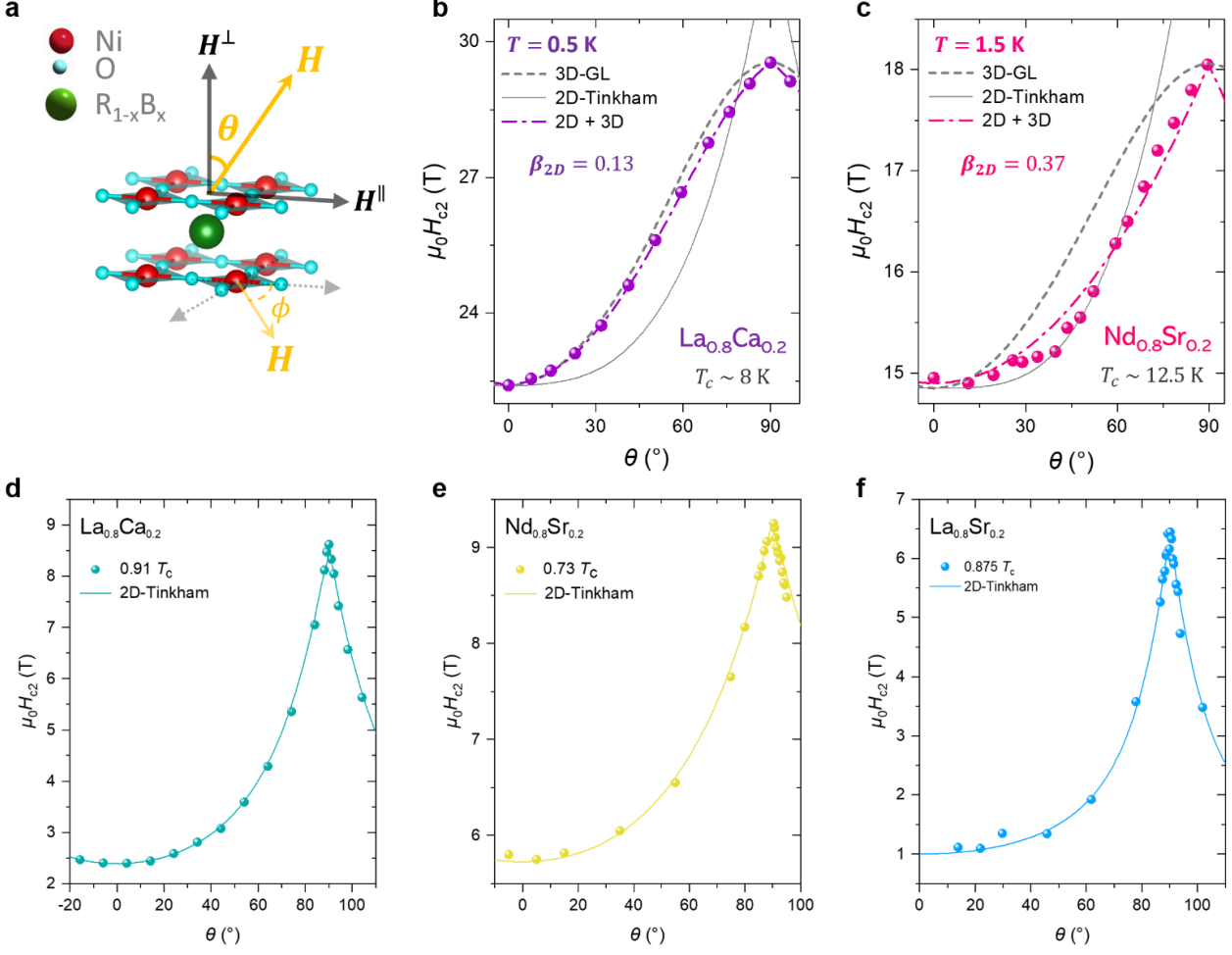


Figure 1: Polar angular-dependent superconducting upper critical fields in layered nickelates.

The definition of field polar angle θ is schematically shown in (a) where $R = La/Nd$, $B = Sr/Ca$. (b-c) $\mu_0 H_{c2}(\theta)$ measured at the lowest temperatures of $\sim 0.06 T_c$ (b) and $\sim 0.12 T_c$ (c) using high pulsed magnetic fields up to 50 T (raw data shown in **Extended Data Fig. 2 & 3**).

(d-f) $\mu_0 H_{c2}(\theta)$ measured near T_c was fitted well to the 2D-Tinkham description. On the other hand, at the lowest temperatures (b-c), $\mu_0 H_{c2}(\theta)$ follows neither a purely 2D-Tinkham nor 3D-GL-like behaviour; instead, we can fit the data to

$$\left[\frac{H_{c2}(\theta) \sin(\theta)}{H_{c2}(90^\circ)} \right]^2 + \alpha_{3D} \left[\frac{H_{c2}(\theta) \cos(\theta)}{H_{c2}(0^\circ)} \right]^2 + \beta_{2D} \left| \frac{H_{c2}(\theta) \cos(\theta)}{H_{c2}(0^\circ)} \right| = 1 \text{ with } \alpha_{3D} + \beta_{2D} = 1.$$

For 2D-Tinkham, $\beta_{2D} = 1, \alpha_{3D} = 0$.

To reveal the temperature evolution of the dimensionality, we compare the $H_{c2}(\theta)$ near T_c with those measured at the lowest possible temperatures of $\sim 0.06 T_c$. In contrast to the near T_c behaviour, the upper critical fields of the Ca-doped LaNiO₂ (**Fig. 1b**) evolve smoothly as a function of angle θ , suggesting a tendency towards a 3D-character at low temperatures. The magnitude of H_{c2} is large and exceeds the Pauli-limit in all directions.¹⁹ As shown in **Figs. 1b-c**, the $H_{c2}(\theta)$ of all systems cannot be fitted to both the 2D-Tinkham model and the 3D anisotropic mass Ginzburg-Landau (GL) model:

$$\left[\frac{H_{c2}(\theta) \sin(\theta)}{H_{c2}(90^\circ)} \right]^2 + \left[\frac{H_{c2}(\theta) \cos(\theta)}{H_{c2}(0^\circ)} \right]^2 = 1.$$

Instead, we fit the $H_{c2}(\theta)$ data to a combined 2D + 3D model:^{36,37}

$$\left[\frac{H_{c2}(\theta) \sin(\theta)}{H_{c2}(90^\circ)} \right]^2 + \alpha_{3D} \left[\frac{H_{c2}(\theta) \cos(\theta)}{H_{c2}(0^\circ)} \right]^2 + \beta_{2D} \left| \frac{H_{c2}(\theta) \cos(\theta)}{H_{c2}(0^\circ)} \right| = 1,$$

which measures the relative dominance of the 2D-Tinkham behaviour (β_{2D}) vs 3D-GL (α_{3D}). We set $\beta_{2D} + \alpha_{3D} = 1$. When $\beta_{2D} \rightarrow 1$, a 2D-Tinkham description is observed. When $\beta_{2D} \rightarrow 0$, a 3D-GL model is fitted. Note that this equation is sensitive to the cusp behaviour near $\theta = 90^\circ$ instead of the general anisotropy γ value. For example, the Sr-doped Nd-nickelate in **Fig. 1e** has a small $\gamma \approx 1.6$, but the sharp peak near $\theta = 90^\circ$ leads to a completely two-dimensional description which the $H_{c2}(\theta)$ is fitted well to the 2D-Tinkham model ($\beta_{2D} = 1$).

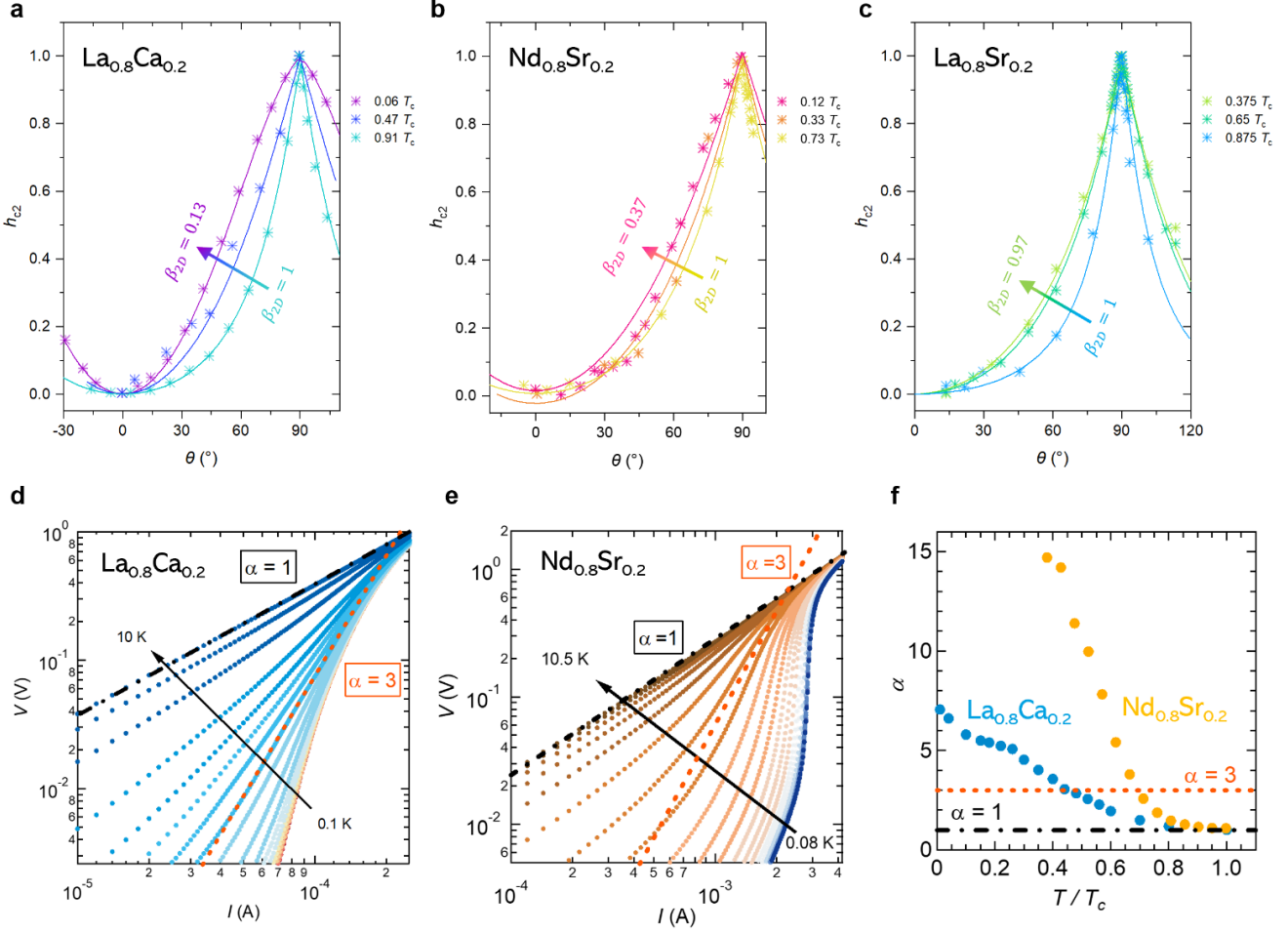


Figure 2: Evidence for dimensionality tuning in infinite-layer nickelates. A crossover from 2D-Tinkham-like to 3D-GL-like superconducting states can be observed in the Ca-doped LaNiO_2 (a) and Sr-doped NdNiO_2 (b). The parameter $h_{c2}(\theta) = \frac{H_{c2}(\theta) - H_{c2}^{\perp}}{H_{c2}^{\parallel} - H_{c2}^{\perp}}$, $0 \leq h_{c2}(\theta) \leq 1$ is used to compare the polar angular dependence of upper critical fields as temperatures lowered towards $T/T_c \rightarrow 0$. (d-f) Evidence for dimensionality control visualised from the BKT transition interpreted from the $I-V$ characteristics at various temperatures down to 0.08 K. When $V \propto I^3$ or $\alpha = 3$, $T_{BKT,(La,Ca)} \sim 0.5 T_c$, $T_{BKT,(Nd,Sr)} \sim 0.7 T_c$, implying that the Sr-doped NdNiO_2 is more two-dimensional-like than the Ca-doped LaNiO_2 , consistent with the $H_{c2}(\theta)$ fitting results (a-c).

Figure 2 summarises the T/T_c evolution of the dimensionality in the layered nickelates family: Ca-doped La-nickelates, Sr-doped La-nickelates, Sr-doped Nd-nickelates. **Figures 2a-c** depict the $H_{c2}(\theta)$ at different T/T_c spanning from near T_c regime to low-temperature regime. To aid the visual comparison, we normalise the vertical axis to $h_{c2}(\theta) = \frac{H_{c2}(\theta) - H_{c2}^\perp}{H_{c2}^\parallel - H_{c2}^\perp}$, where $0 \leq h_{c2}(\theta) \leq 1$. One can see the striking differences in the dimensionality evolution in various rare-earth (La/Nd) and hole dopant (Sr/Ca) systems. For the Ca-doped La-nickelates (**Fig. 2a**), the $H_{c2}(\theta)$ evolves from a cusp-like peak near $\theta = 90^\circ$ at temperatures near T_c to a smooth peak at the lowest temperature of $0.06 T_c$, demonstrating the ‘2D-ness’ $\beta_{2D} = 1 \rightarrow \beta_{2D} = 0.13$ as $T \rightarrow 0$. Additional $H_{c2}(\theta)$ data is presented in **Extended Data Fig. 5**. However, for larger dopant size Sr^{2+} as compared to the rare-earth ions, the Sr-doped system has a far stronger two-dimensional character in the superconducting states at the lowest temperature; for the Sr-doped LaNiO_2 (**Fig. 2c**), $H_{c2}(\theta)$ at temperature down to $0.375 T_c$ still can be fully captured by the 2D-Tinkham behaviour. A consistent trend in the ‘2D-ness’ of various rare-earth and hole dopant-based nickelates can be observed in the Berezinskii–Kosterlitz–Thouless (BKT) description of 2D superconductivity from the current-voltage characteristic plotted in logarithmic scale in **Figs. 2d-e**. The BKT transition can be taken at $\alpha = 3$ in $V \propto I^\alpha$. As shown in **Fig. 2f**, the Sr-doped NdNiO_2 still presents a relatively significant change in α as compared to the Ca-doped LaNiO_2 despite having a smaller NiO_2 plane separation (**Fig. 3**), and a defined T_{BKT} closer to the T_c , which suggests the strong influence of dopant size (large Sr^{2+} as compared to the rare-earth ions) in controlling the dimensionality in layered nickelates.

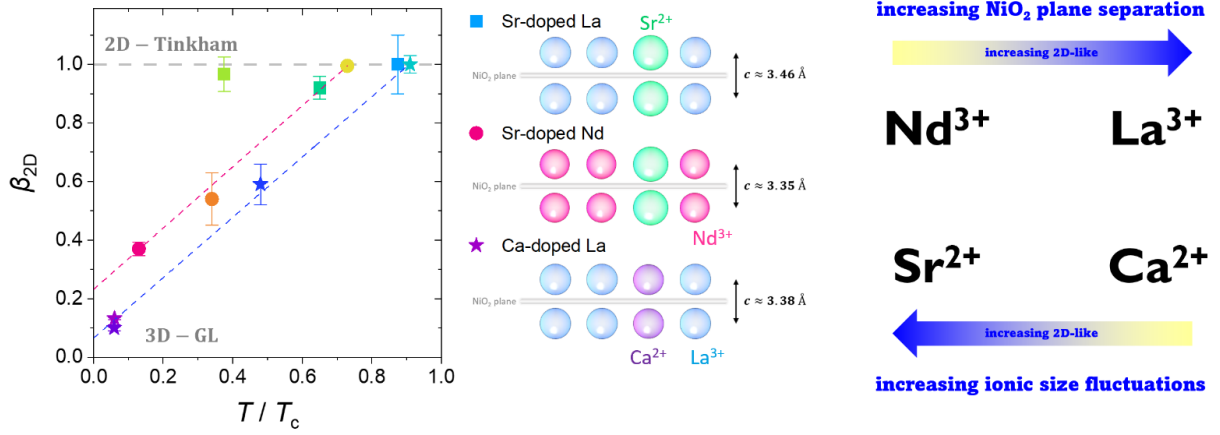


Figure 3: Role of the rare-earth ions Nd^{3+} , La^{3+} and hole dopants Sr^{2+} , Ca^{2+} in controlling the dimensionality of infinite-layer nickelates. The left figure plotted the fitted β_{2D} value from $H_{c2}(\theta)$ of $\text{La}_{0.8}\text{Sr}_{0.2}$ (square), $\text{Nd}_{0.8}\text{Sr}_{0.2}$ (circle), $\text{La}_{0.8}\text{Ca}_{0.2}$ (star) at different T/T_c down to the 0 K limit. The red and blue linear dashed lines are fitted to $\beta_{2D}\left(\frac{T}{T_c}\right) = \beta_0 + \beta'\left(\frac{T}{T_c}\right)$. At $T \rightarrow 0$ K limit, $\beta_0^{\text{LaCa}} = 0.066$, $\beta_0^{\text{NdSr}} = 0.23$. The small $\beta_0 \rightarrow 0$ suggests a dominant 3D-character of superconductivity. The slope $\beta' \sim 1$. While Ca-doped LaNiO_2 has a larger NiO_2 plane separation ($c \approx 3.38$ Å) than the Sr-doped NdNiO_2 ($c \approx 3.35$ Å), Ca-doped LaNiO_2 exhibits more 3D-like character at the lowest temperature suggesting the strong influence of ionic size fluctuations in the rare-earth spacer layer caused by hole dopants doped into the A -site layer. The middle panel depicts a schematic illustration of the ionic size fluctuations with A -site ions and c -axis lattice constant (= NiO_2 plane separation) drawn to scale: $r^{\text{La}^{3+}} \sim 117$, $r^{\text{Nd}^{3+}} \sim 112$, $r^{\text{Ca}^{2+}} \sim 114$, $r^{\text{Sr}^{2+}} \sim 132$ pm.

We summarise the 2D-to-3D dimensional crossover in the superconductivity of infinite-layer nickelates in **Fig. 3** and correspond the observation to the NiO_2 plane separation and the ionic size fluctuations in the rare-earth spacer layer caused by the size of the hole dopants Sr^{2+} , Ca^{2+} . The β_{2D} value tracks the ‘2D-ness’ of various nickelates. The first hypothesis should be the larger the NiO_2 plane separation, the more two-dimensional-like superconductivity in layered nickelates. This hypothesis is valid when comparing La-nickelate (larger $c \approx 3.46$ Å) and Nd-

nickelate ($c \approx 3.35 \text{ \AA}$) with the same hole dopant Sr^{2+} , where the Sr-doped La-nickelate remains purely two-dimensional at $\sim 0.38 T_c$, while the Sr-doped Nd-nickelate has $\beta_{2D} \approx 0.6$, demonstrating a transition to partially three-dimensional in the superconducting coherence. However, when a smaller Ca^{2+} is doped into the rare-earth spacer layer, even though the Ca-doped La-nickelate has a larger NiO_2 plane separation than the Sr-doped Nd-counterpart, superconductivity in the Ca-doped La-nickelate appears to be more three-dimensional in both the $H_{c2}(\theta)$ behaviour near $\theta = 90^\circ$ and $I - V$ characteristic. Here we note that the conclusion of 2D-to-3D dimensional crossover superconductivity is consistent with the interpretation from the superfluid density near T_c behaviour.¹⁸

We propose that while the first picture of increasing the NiO_2 plane separation can lead to a stronger two-dimensional character, the key to tuning the superconductivity in layered nickelates to be two-dimensional like the high- T_c cuprates lies in modifying the spacer layer, where increasing the ionic size fluctuations in the rare-earth spacer layer can dramatically change the dimensionality of superconductivity in nickelates. With this observation, we can speculate that the Ba-doped LaNiO_2 is a purely two-dimensional superconductor with the highest hope of achieving cuprates-like pairing in infinite-layer nickelates. On the other hand, one can boost the 3D character and the corresponding responsible pairing mechanism by synthesizing Ca-doped NdNiO_2 , which should carry the strongest 3D-like and potentially nodeless superconductivity in the layered nickelates family. The present work resolves the longstanding debates on whether nickelates' superconductivity is two-dimensional or three-dimensional and proposes that layered nickelates are the ideal platform to manipulate dimensionality and study the relationship between reduced dimensionality and superconducting pairing mechanism.

Broken rotational symmetry in the superconducting states

The anisotropy of the superconductivity in the square-planar NiO₂ planes was investigated by probing the change in the superconducting observables: (1) the superconducting critical current $I_c[B^\parallel(\phi)]$, which is related to the superconducting gap, (2) the fraction of the superconducting state relative to the normal state visualised in $\rho[B^\parallel(\phi)]$ within the superconducting transition, upon applying an in-plane magnetic field B^\parallel along different directions ϕ . **Figures 4a,d** show the in-plane azimuthal angular dependent $I_c[B^\parallel(\phi)]$ at temperatures from ~ 0.1 K to ~ 5 K in the Nd-nickelate Nd_{0.8}Sr_{0.2}NiO₂ and La-nickelate La_{0.8}Ca_{0.2}NiO₂. In both Nd- and La-nickelates, we see a two-fold modulation of the I_c , which breaks the four-fold C_4 rotational symmetry of the square-planar NiO₂ lattice structure. In the Nd-nickelates, in addition to the C_2 symmetric component, a C_4 symmetric component is present. To decouple the C_2 vs C_4 contributions, we fitted the $I_c[B^\parallel(\phi)]$ data to

$$A_{C_2} \sin(2(\phi - \phi_{C_2})) + A_{C_4} \sin(4(\phi - \phi_{C_4})) + A$$

as shown in the grey dashed lines. For La-nickelate, only the C_2 symmetric component is necessary to describe the in-plane variation in $I_c[B^\parallel(\phi)]$. For Nd-nickelate, we can fit the data to a significant C_4 component. The four-fold contributions exist at a broad temperature range but increase as temperature decreases from 5.5 to 0.15 K. Such temperature dependence of the C_4 rotational symmetry for the Nd-nickelates only can most naturally be explained as the orientation of the Nd³⁺ 4*f* moments.

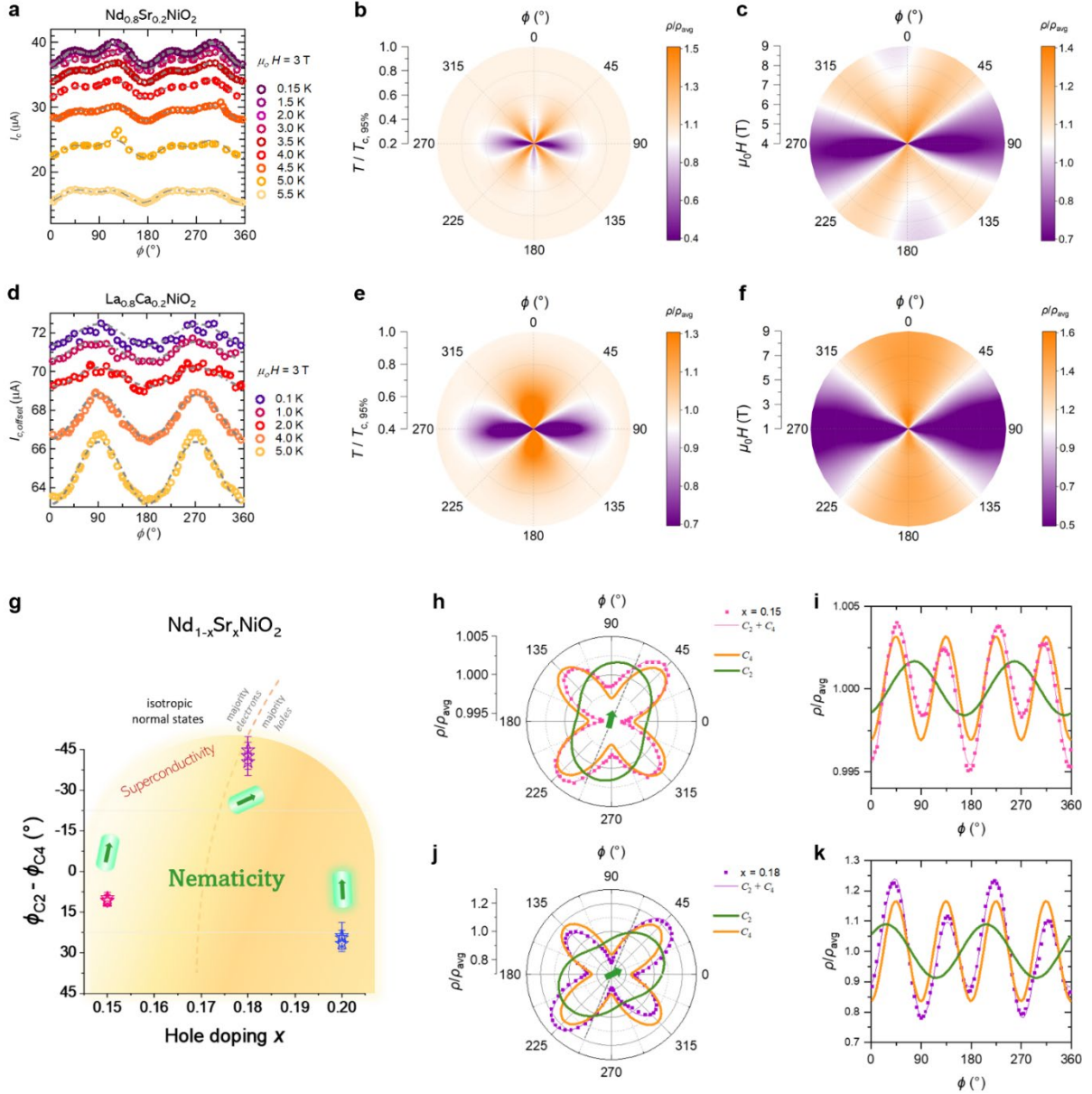


Figure 4: Evidence for (in-plane) anisotropic superconducting observables in square-planar nickelates. Representative Nd-nickelates $\text{Nd}_{0.8}\text{Sr}_{0.2}\text{NiO}_2$ (**a-c**) and La-nickelates $\text{La}_{0.8}\text{Ca}_{0.2}\text{NiO}_2$ (**d-f**). (**Top left: a,d**) Modulation of the superconducting critical current I_c as a function of in-plane field B^{\parallel} orientation measured using a 2D-vector magnet. Data for La-nickelate (**d**) are offset vertically for clarity. Sinusoidal functions of $C_2 + C_4$ symmetry $A_{C_2} \sin(2(\phi - \phi_{C_2})) + A_{C_4} \sin(4(\phi - \phi_{C_4}))$ show a good fit to the Nd-nickelate $I_c[B^{\parallel}(\phi)]$ (**a**) and magnetoresistance $\rho[B^{\parallel}(\phi)]$ within superconducting transition (**h-k**), while only a C_2 symmetry term is needed to describe the anisotropic $I_c[B^{\parallel}(\phi)]$ of La-nickelate (**d**). (**b-c, e-f**) Polar maps (in-plane azimuthal angle of B^{\parallel}) of the anisotropic

magnetoresistance at different temperatures $T/T_{c,95\%}$ (**b,e**) and different magnitudes of B^{\parallel} (**c,f**). Data were measured at 9 T (**b,e**) and $\sim 0.5 T/T_{c,95\%}$ (**c,f**). For La-nickelate (**d-f**), only a C_2 symmetry was observed in the superconducting state. (**g-k**) Hole doping dependence of the C_2 symmetry phase shift ϕ_{C_2} with respect to ϕ_{C_4} in $\text{Nd}_{1-x}\text{Sr}_x\text{NiO}_2$. Data for representative $x = 0.15$ (**h-i**) was measured at 9 K with $B^{\parallel} = 9$ T, $x = 0.18$ (**j-k**) was measured at 2 K with $B^{\parallel} = 4$ T.

We further investigate the consistency of the observation of anisotropic superconducting critical current by measuring the in-plane angular dependent $\rho[B^{\parallel}(\phi)]$ within the superconducting transition. To determine if there is any anisotropic contribution from the normal state electrons, we measure the azimuthal angular-dependent magnetoresistance at a temperature above T_c or sufficiently large magnetic field to be in the normal state as shown in **Extended Data Figs. 6a-f**. The normal state azimuthal angular dependent magnetoresistance shows virtually a circle in the polar plot with negligible anisotropy being observed. Therefore, we can exclude the trivial contribution of normal state electrons in the $\rho[B^{\parallel}(\phi)]$ within the superconducting transition and observe only the anisotropy in the superconducting states. **Extended Data Figs. 6d-k** show the in-plane azimuthal angular dependent $\rho[B^{\parallel}(\phi)]$ for $\text{Nd}_{1-x}\text{Sr}_x\text{NiO}_2$, $\text{La}_{1-x}\text{Ca}_x\text{NiO}_2$, and $\text{La}_{1-x}\text{Sr}_x\text{NiO}_2$ square-planar nickelates family. For La-nickelates, we can see a clear two-fold pattern in the superconducting states presented as an oval- or infinity-shape in the polar plot. For Nd-nickelate, an additional four-fold component is present at all hole doping x , which manifests as a cloverleaf pattern. The anisotropic $\rho[B^{\parallel}(\phi)]$ is summarised in the polar maps in **Figs. 4b-c** for $C_2 + C_4$ symmetry in Nd-nickelates, and **Figs. 4e-f** for C_2 symmetry in the La-nickelates.

Next, we investigate the relationship between the C_2 symmetric component and the C_4 symmetric component in the Nd-nickelates in terms of the phase shift $\phi_{C_2} - \phi_{C_4}$. The same forms of the sinusoidal functions are used in the fitting as previously discussed for the $I_c[B^\parallel(\phi)]$. As shown in the fitting results for representative hole doping levels $x = 0.15$ (**Figs. 4h-i**) and $x = 0.18$ (**Figs. 4j-k**), the phase shift for C_2 symmetric component is different for different doping levels, as visualised in the green arrow in **Figs. 4g-h & j**, which can be interpreted as the C_2 symmetric director rotated as hole doping crossing the majority electrons – majority holes transition (sign reversal in the Hall coefficients) in the superconducting dome of hole-doped Nd-nickelates.

Before we discuss the interpretation of the C_2 symmetric anisotropy in the family of square-planar nickelates, we first rule out a few trivial explanations for the observation. First, we performed the measurement in a different current direction $\phi_{\vec{I}}$ and see if the C_2 symmetric component shifted with phase $\phi_{\vec{I}}$ on the same sample. As shown in **Extended Data Fig. 7**, the representative top panel data is measured at $\phi_{\vec{I}} = 0^\circ$ while the bottom panel data is measured at $\phi_{\vec{I}} = 45^\circ$ at 9 T magnetic field in $\text{Nd}_{0.8}\text{Sr}_{0.2}\text{NiO}_2$. We can see the two-fold pattern in the bottom panel did not shift by $\phi_{\vec{I}} = 45^\circ$ with the current direction. Therefore, we can rule out Lorentz effect on the current as the cause of C_2 symmetric anisotropy. Secondly, we can exclude sample tilt as an explanation for the C_2 symmetric anisotropy. As shown in **Extended Data Fig. 8**, for the same sample mounted with the same in-plane orientation but intentionally tilted to a small angle of $\theta_{\text{tilt}} \sim 10^\circ$, the measured azimuthal angular dependent $\rho[B^\parallel(\phi)]$ pattern is completely changed to two sharp dips at $\phi_{\text{dip}} \sim 162^\circ$ and $\phi_{\text{dip}} \sim 342^\circ$, which are at a different position from the original two-fold minima positions. In addition, as we discussed in the polar angular dependent $H_{C_2}(\theta)$, at low temperatures, the H_{C_2} variation near the in-plane direction $H_{C_2}^\parallel$ is smooth, and the superconducting state is mostly three-dimensional. Therefore,

any small potential misalignment in the experiments would have a negligible effect on the in-plane anisotropy.

The observed C_2 rotational symmetry in the family of square-planar nickelates would suggest a rotational-symmetry-breaking superconducting state that is unexpected from the four-fold symmetry of the lattice structure, which could be interpreted as nematicity. Such nematic superconductivity is different from the nematicity observed in the normal state of electrons in the strongly-correlated system such as iron-based superconductor,³⁸ layered ruthenates Sr_2RuO_4 and $\text{Sr}_3\text{Ru}_2\text{O}_7$,^{39,40} heavy-fermion URu_2Si_2 ,⁴¹ and in the high- T_c cuprates.^{42,43} Considering nickelate is designed as a cuprate-analogue, it may not be surprising to find nematicity in the square-planar nickelates. We remain cautious to note that, if the hole dopants $\text{Sr}^{2+}/\text{Ca}^{2+}$ form a particular ordering upon substitution of the rare-earth ions, such superlattice structure (for example a chain) may potentially lead to some anisotropies in both the normal state and superconducting state. However, we did not observe any anisotropy in the normal state. Similar rotational symmetry breaking superconductivity was proposed in the flat-band twisted-bilayer-graphene,⁴⁴ few-layer NbSe_2 ,⁴⁵ and $\text{Cu}_x\text{Bi}_2\text{Se}_3$.⁴⁶ Nematic superconductivity is associated with the two-dimensional E representation with odd parity p -wave pairing which should possess topological nature that is different from the B representation for d -wave in cuprates. Interestingly, unlike cuprates, the additional contribution from the Ni d_{z^2} flat-band in nickelates favour spin-triplet p -wave pairing,²⁸ that was proposed theoretically to be significant at a sufficient hole doping level which can be observed in the superconducting dome given the self-doping effect. On the other hand, another calculation based on density functional theory (DFT) + many-body perturbation theory proposed that even undoped nickelates have prominent d_{z^2} flat-band near the Fermi level which can give rise to van Hove singularities in the density of states and electronic nematicity.⁴⁷ The next question is how does the (gap/spin/electronic) nematicity interacts with the superconductivity especially near the

quantum critical point (if exists) of the strongly-correlated hole-doped nickelates, which will be relevant for the pairing mechanism and order parameters of this newfound family of superconductors.

Note: During the preparation of this manuscript, we became aware of two reports on the in-plane magnetoresistance anisotropy,^{48,49} and one report on the $T_c(\theta)$ in Sr-doped La-nickelate.⁵⁰

References

1. Anderson, P. W. *Basic Notions Of Condensed Matter Physics*. (Westview Press, 1997).
2. Chiu, C.-K., Teo, J. C. Y., Schnyder, A. P. & Ryu, S. Classification of topological quantum matter with symmetries. *Rev. Mod. Phys.* **88**, 035005 (2016).
3. Rice, T. M. Electronic structure of possible nickelate analogs to the cuprates. *Phys. Rev. B - Condens. Matter Mater. Phys.* **59**, 7901–7906 (1999).
4. Lee, K. W. & Pickett, W. E. Infinite-layer LaNiO₂: Ni¹⁺ is not Cu²⁺. *Phys. Rev. B - Condens. Matter Mater. Phys.* **70**, 1–7 (2004).
5. Li, D. *et al.* Superconductivity in an infinite-layer nickelate. *Nature* **572**, 624–627 (2019).
6. Zeng, S. *et al.* Phase Diagram and Superconducting Dome of Infinite-Layer Nd_{1-x}Sr_xNiO₂ Thin Films. *Phys. Rev. Lett.* **125**, 147003 (2020).
7. Zeng, S. *et al.* Superconductivity in infinite-layer nickelate La_{1-x}Ca_xNiO₂ thin films. *Sci. Adv.* **8**, eabl9927 (2022).
8. Pan, G. A. *et al.* Superconductivity in a quintuple-layer square-planar nickelate. *Nat. Mater.* **21**, 160–164 (2022).
9. Bednorz, J. G., Takashige, M. & Müller, K. A. Possible high-T_c superconductivity in the Ba-La-Cu-O system. *Z. Phys. B* **64**, 189–193 (1986).
10. Anderson, P. W. *The Theory of Superconductivity in the High-T_c Cuprate Superconductors*. (Princeton University Press, 1997).
11. Maeno, Y. *et al.* Superconductivity in a layered perovskite without copper. *Nature* **372**, 532–534 (1994).
12. Takada, K. *et al.* Superconductivity in two-dimensional CoO₂ layers. *Nature* **422**, 53–55 (2003).

13. Chen, X. H. *et al.* Superconductivity at 43 K in $\text{SmFeAsO}_{1-x}\text{F}_x$. *Nature* **453**, 761–762 (2008).
14. Osada, M. *et al.* Nickelate Superconductivity without Rare-Earth Magnetism: $(\text{La,Sr})\text{NiO}_2$. *Adv. Mater.* **33**, 1–23 (2021).
15. Hepting, M. *et al.* Electronic structure of the parent compound of superconducting infinite-layer nickelates. *Nat. Mater.* **19**, 381–385 (2020).
16. Lu, H. *et al.* Magnetic excitations in infinite-layer nickelates. *Science* **216**, 213–216 (2021).
17. Kitatani, M. *et al.* Nickelate superconductors—a renaissance of the one-band Hubbard model. *npj Quantum Mater.* **5**, 6–11 (2020).
18. Chow, L. E. *et al.* Pairing symmetry in infinite-layer nickelate superconductor. Preprint at <https://arxiv.org/abs/2201.10038> (2022).
19. Chow, L. E. *et al.* Pauli-limit violation in lanthanide infinite-layer nickelate superconductors. Preprint at <https://arxiv.org/abs/2204.12606> (2022).
20. Chow, L. E. & Ariando, A. Infinite-Layer Nickelate Superconductors: A Current Experimental Perspective of the Crystal and Electronic Structures. *Front. Phys.* **10**, (2022).
21. Nomura, Y. & Arita, R. Superconductivity in infinite-layer nickelates. *Reports Prog. Phys.* **85**, 052501 (2022).
22. Been, E. *et al.* Electronic Structure Trends Across the Rare-Earth Series in Superconducting Infinite-Layer Nickelates. *Phys. Rev. X* **11**, 1–14 (2021).
23. Botana, A. S., Bernardini, F. & Cano, A. Nickelate Superconductors: An Ongoing Dialog between Theory and Experiments. *J. Exp. Theor. Phys.* **132**, 618–627 (2021).
24. Martínez, J. C. *et al.* Magnetic anisotropy of a $\text{Bi}_2\text{Sr}_2\text{CaCu}_2\text{O}_x$ single crystal. *Phys. Rev. Lett.* **69**, 2276–2279 (1992).
25. Yu, Y. *et al.* High-temperature superconductivity in monolayer $\text{Bi}_2\text{Sr}_2\text{CaCu}_2\text{O}_{8+\delta}$. *Nature* **575**, 156–163 (2019).
26. Yuan, H. Q. *et al.* Nearly isotropic superconductivity in $(\text{Ba,K})\text{Fe}_2\text{As}_2$. *Nature* **457**, 565–568 (2009).
27. Jiang, M., Berciu, M. & Sawatzky, G. A. Stabilization of singlet hole-doped state in infinite-layer nickelate superconductors. *Phys. Rev. B* **106**, 115150 (2022).
28. Kreisel, A., Andersen, B. M., Rømer, A. T., Eremin, I. M. & Lechermann, F. Superconducting Instabilities in Strongly Correlated Infinite-Layer Nickelates. *Phys. Rev. Lett.* **129**, 077002 (2022).
29. Held, K. *et al.* Phase Diagram of Nickelate Superconductors Calculated by Dynamical Vertex Approximation. *Front. Phys.* **9**, (2022).
30. Worm, P. *et al.* Correlations tune the electronic structure of pentalayer nickelates into the superconducting

- regime. *Phys. Rev. Mater.* **6**, L091801 (2022).
31. LaBollita, H. & Botana, A. S. Correlated electronic structure of a quintuple-layer nickelate. *Phys. Rev. B* **105**, 085118 (2022).
 32. Keimer, B., Kivelson, S. A., Norman, M. R., Uchida, S. & Zaanen, J. From quantum matter to high-temperature superconductivity in copper oxides. *Nature* **518**, 179–186 (2015).
 33. Krieger, G. *et al.* Charge and Spin Order Dichotomy in NdNiO₂ Driven by the Capping Layer. *Phys. Rev. Lett.* **129**, 027002 (2022).
 34. Rossi, M. *et al.* A broken translational symmetry state in an infinite-layer nickelate. *Nat. Phys.* **18**, 869–873 (2022).
 35. Tam, C. C. *et al.* Charge density waves in infinite-layer NdNiO₂ nickelates. *Nat. Mater.* **21**, 1116–1120 (2022).
 36. Goh, S. K. *et al.* Anomalous Upper Critical Field in CeCoIn₅/YbCoIn₅ Superlattices with a Rashba-Type Heavy Fermion Interface. *Phys. Rev. Lett.* **109**, 157006 (2012).
 37. Shimozawa, M. *et al.* Controllable Rashba Spin-Orbit Interaction in Artificially Engineered Superlattices Involving the Heavy-Fermion Superconductor CeCoIn₅. *Phys. Rev. Lett.* **112**, 156404 (2014).
 38. Kasahara, S. *et al.* Electronic nematicity above the structural and superconducting transition in BaFe₂(As_{1-x}P_x)₂. *Nature* **486**, 382–385 (2012).
 39. Borzi, R. A. *et al.* Formation of a Nematic Fluid at High Fields in Sr₃Ru₂O₇. *Science* **315**, 214–217 (2007).
 40. Wu, J. *et al.* Electronic nematicity in Sr₂RuO₄. *Proc. Natl. Acad. Sci.* **117**, 10654–10659 (2020).
 41. Okazaki, R. *et al.* Rotational Symmetry Breaking in the Hidden-Order Phase of URu₂Si₂. *Science* **331**, 439–442 (2011).
 42. Daou, R. *et al.* Broken rotational symmetry in the pseudogap phase of a high-T_c superconductor. *Nature* **463**, 519–522 (2010).
 43. Wu, J., Bollinger, A. T., He, X. & Božović, I. Spontaneous breaking of rotational symmetry in copper oxide superconductors. *Nature* **547**, 432–435 (2017).
 44. Cao, Y. *et al.* Nematicity and competing orders in superconducting magic-angle graphene. *Science* **372**, 264–271 (2021).
 45. Hamill, A. *et al.* Two-fold symmetric superconductivity in few-layer NbSe₂. *Nat. Phys.* **17**, 949–954 (2021).
 46. Yonezawa, S. *et al.* Thermodynamic evidence for nematic superconductivity in Cu_xBi₂Se₃. *Nat. Phys.* **13**, 123–126 (2017).
 47. Zhang, R. *et al.* Fingerprints of nematicity and competing orders in the infinite-layer nickelate. Preprint at <https://arxiv.org/abs/2207.00184> (2022).

48. Wang, B. Y. *et al.* Rare-Earth Control of the Superconducting Upper Critical Field in Infinite-Layer Nickelates. Preprint at <https://arxiv.org/abs/2205.15355> (2022).
49. Ji, H. *et al.* Rotational symmetry breaking in superconducting nickelate $\text{Nd}_{0.8}\text{Sr}_{0.2}\text{NiO}_2$ films. Preprint at <https://arxiv.org/abs/2210.17023> (2022).
50. Sun, W. *et al.* Evidence for quasi-two-dimensional superconductivity in infinite-layer nickelates. Preprint at <https://arxiv.org/abs/2204.13264> (2022).

Methods

Sample growth and preparation

The infinite-layer nickelates $\text{Nd}_{1-x}\text{Sr}_x\text{NiO}_2$ and $\text{La}_{1-x}(\text{Ca}/\text{Sr})_x\text{NiO}_2$ thin films were grown on SrTiO_3 (001) substrates using pulsed laser deposition and CaH_2 topotactic reduction process under conditions as previously reported.¹⁸ The electron microscopy (STEM annular bright field and high-angle annular dark field) and electron energy loss spectroscopy characterisation are shown in **Extended Data Fig. 1**.

Polar and Azimuthal angular-dependent magnetotransport measurement

The wire connection for the electrical transport measurement was made by Al ultrasonic wire bonding. The transport measurements at temperatures down to 2 K or in magnetic field up to 14 T were performed using a Quantum Design Physical Property Measurement System with a rotator with an angle range from -10° to 370° . The onset of transitions $T_{c,95\%}$ is defined as the temperature at which the resistivity value reaches 95% of resistivity at 20 K, ρ_{20K} . Unless otherwise specified, T_c and H_{c2} in this article denotes the 50% resistivity transition criteria.

High magnetic pulsed-field transport measurement

The polar θ angular dependent of the upper critical fields (and magnetoresistance) were measured in pulsed-field $^3\text{He}/^4\text{He}$ -cryostats. The La-nickelates were measured in magnetic field strength up to 65 T (~ 80 ms) and at temperatures down to ~ 0.5 K at the pulsed field

facility of NHMFL in Los Alamos. The Nd-nickelates were measured in LNCMI-Toulouse with field strength up to 55 T (~ 300 ms) and temperature down to ~ 1.5 K.

In-plane angular dependent superconducting critical current measurement

The $I - V$ characteristics of the superconducting nickelates were measured in a ^3He - ^4He Bluefors LD250 dilution fridge with a base temperature of < 10 mK. To avoid sizeable Joule heating due to transport current, the critical current measurements were conducted at a temperature above 80 mK, where the dilution fridge has a cooling power of at least $160 \mu\text{W}$. The dilution fridge is equipped with a two-dimensional vector magnet with a rotatable field of 3 T. To extract the azimuthal ϕ angular dependent of the superconducting critical current $I_c[B^\parallel(\phi)]$ under an in-plane magnetic field, we first measure the $I - V$ curves at a series of various angle ϕ , temperature, and field magnitude (e.g. $\phi = 12^\circ, T = 0.1$ K, $B = 3$ T), then plot dV/dI vs I , and extract I_c using 5% transition criteria.

Data availability

The data that support the findings of this study are available from the corresponding author upon reasonable request.

Competing interest declaration

The authors declare no competing financial interests.

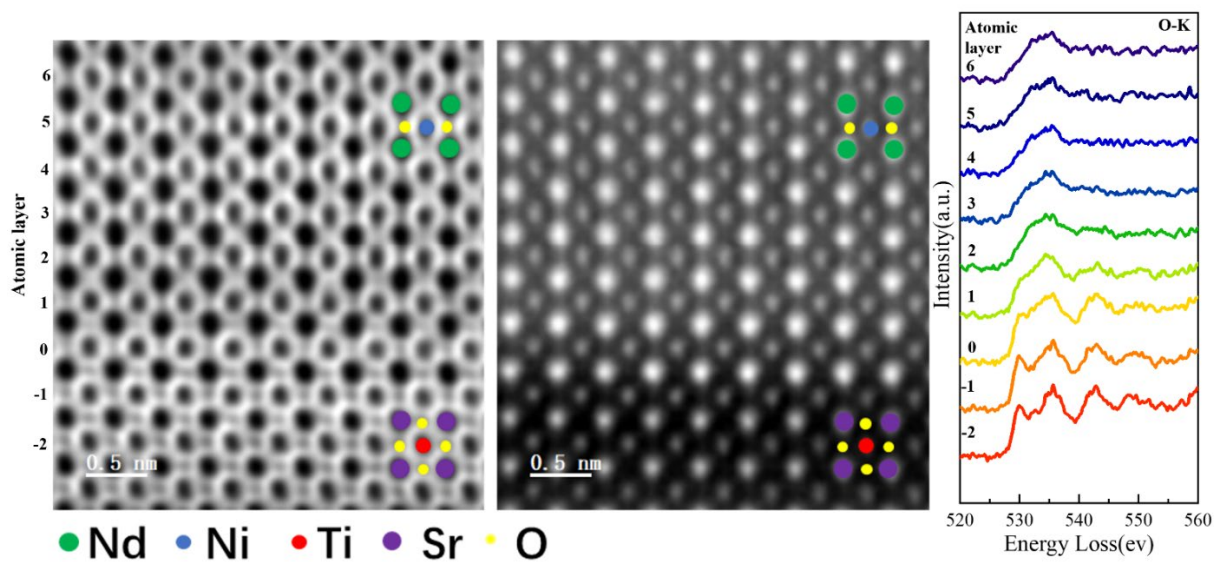
Authors contribution

A.A. conceived and led the project. L.E.C., K.R., K.Y.Y., W.E., S.K.G., and A.A. designed the experiments. L.E.C., S.W.Z., Z.Y.L. synthesized the infinite-layer nickelate thin films. K.R. and N.H. measured the angular-dependent upper critical fields of $\text{La}_{0.8}\text{Ca}_{0.2}\text{NiO}_2$ at temperatures below 4.2 K in high magnetic fields. The pulsed field data of $\text{Nd}_{0.8}\text{Sr}_{0.2}\text{NiO}_2$ was measured by M.P., M.L., M.G., and W.E. The anisotropic superconducting critical current data was measured by K.Y.Y., X.Y.L. and S.W.G. The polar and azimuthal angular dependent magnetoresistance data was measured by L.E.C. with K.Y.Y.. Z.Y.L. and C.L. performed the electron microscopy and spectroscopy analysis. L.E.C. and A.A. analysed the data and wrote the manuscripts with input from all authors.

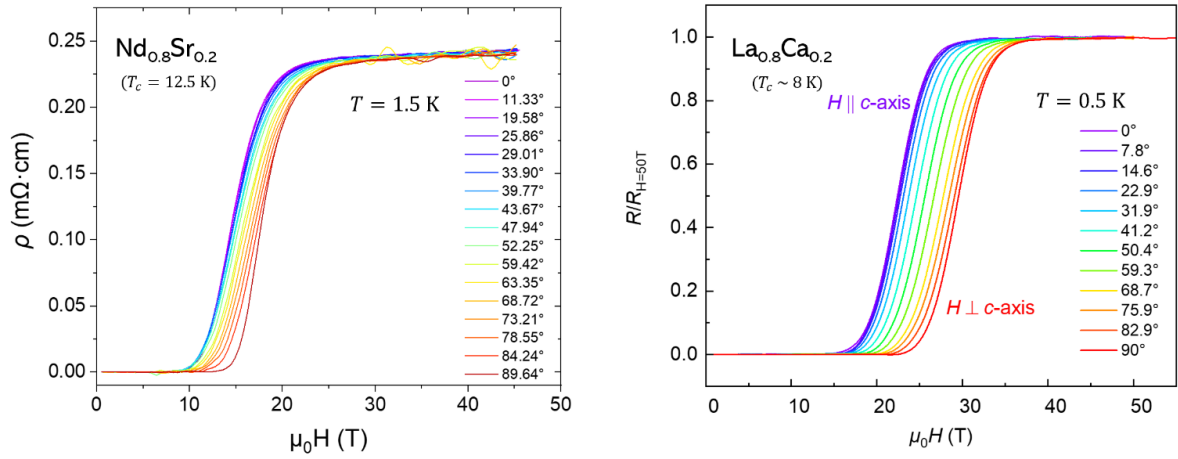
Acknowledgement

We acknowledge the helpful discussions with Hiroshi Yamase, Liang Si, and Karsten Held. This research is supported by the Ministry of Education (MOE), Singapore, under its Tier-2 Academic Research Fund (AcRF), Grant No. MOET2EP50121-0018, and Research Grants Council of the Hong Kong SAR, Grant No. A-CUHK 402/19. We acknowledge the support of LNCMI-CNRS, a member of the European Magnetic Field Laboratory (EMFL) under the proposal numbers TMS03-122 and TMS04-122. The research at NHMFL is supported by the National Science Foundation through NSF/DMR-1644779 and the State of Florida, the US Department of Energy “Science of 100 Tesla” BES program, and the Laboratory Directed Research and Development program of Los Alamos National Laboratory under project 20210320ER.

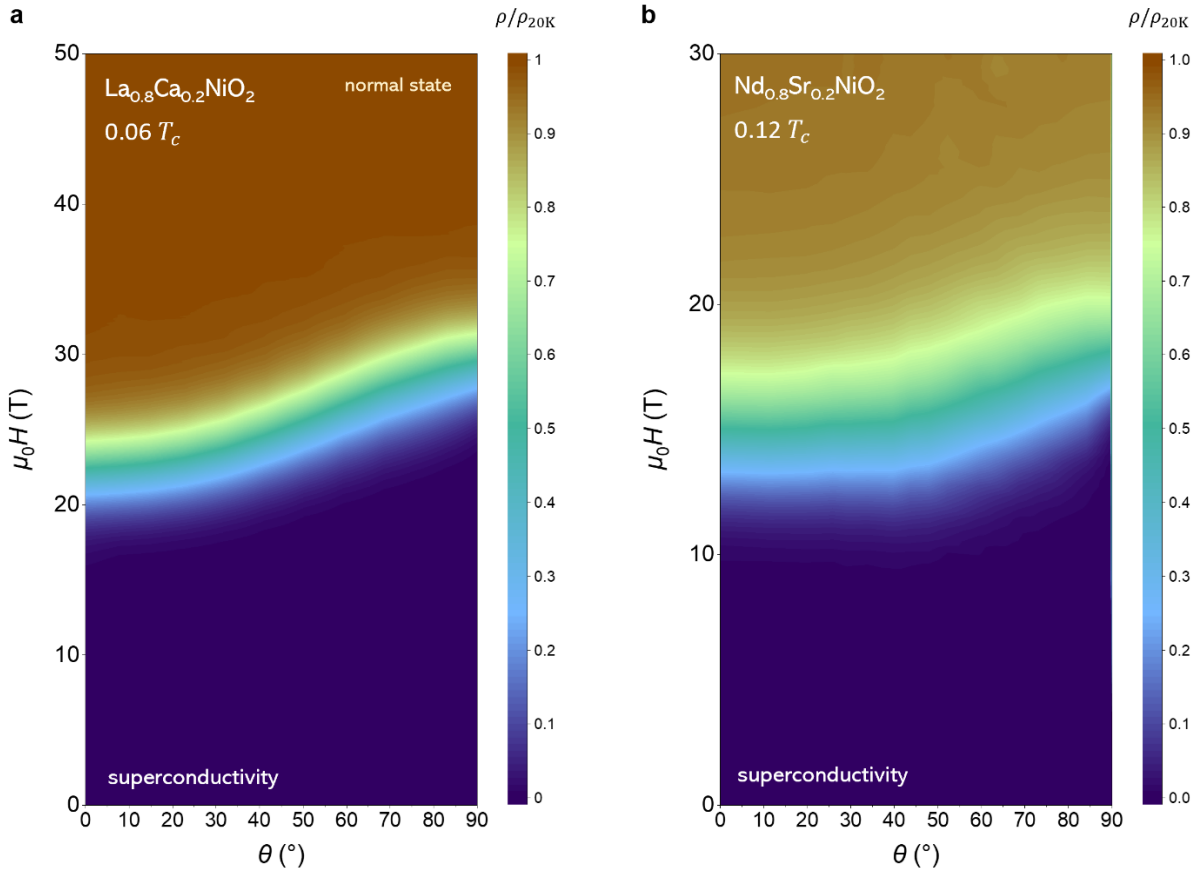
Extended Data



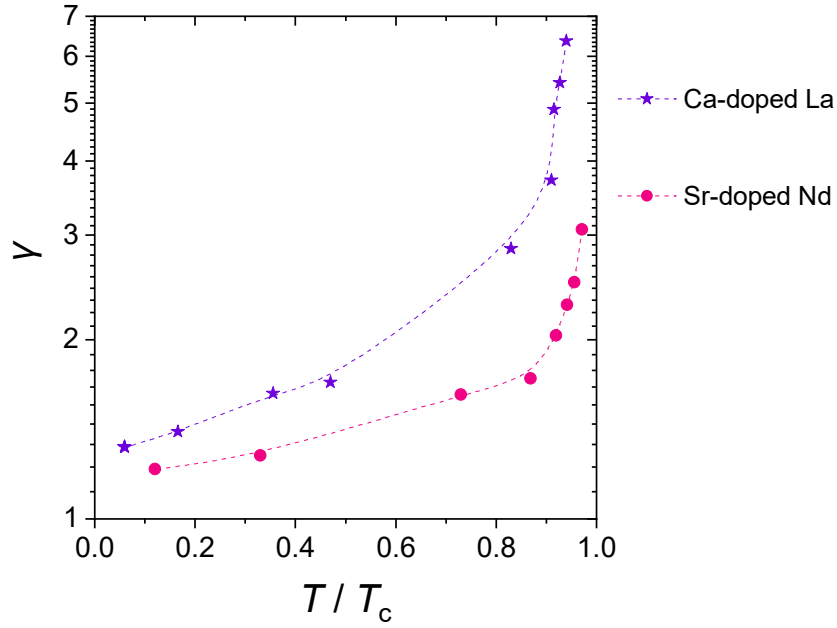
Extended Data Figure 1: Electron microscopy and spectroscopy analysis of a representative infinite-layer nickelates $\text{Nd}_{0.8}\text{Sr}_{0.2}\text{NiO}_2$. The interface layer between nickelates and $\text{SrTiO}_3(001)$ substrate is denoted as layer '0'. From left to right: the annular-bright-field (ABF-STEM), high-angle annular dark-field (HAADF-STEM), and electron energy loss spectroscopy (EELS) at O *K* edge.



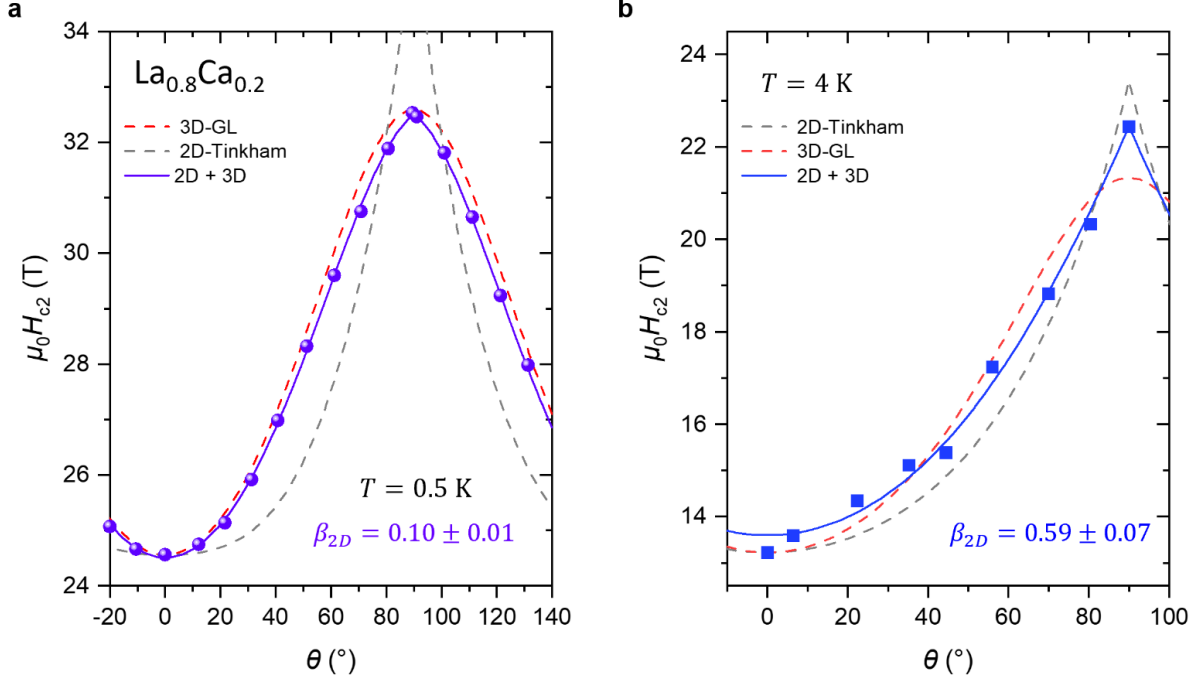
Extended Data Figure 2: Magnetoresistance measured in high-magnetic pulsed-field setup at different polar angles θ . Representative low-temperature $R - H$ curves at different polar angles θ with respect to the out-of-plane (\perp NiO_2 plane) direction for $\text{Nd}_{0.8}\text{Sr}_{0.2}\text{NiO}_2$ (**left**) and $\text{La}_{0.8}\text{Ca}_{0.2}\text{NiO}_2$ (**right**).



Extended Data Figure 3: $H - \theta$ maps of the magnetoresistance measured in high-magnetic pulsed-field setup at different polar angles θ . Data is mapped with $R - H$ curves (shown in **Extended Data Fig. 2**) at different polar angles θ with respect to the out-of-plane (\perp NiO_2 plane) direction for $\text{La}_{0.8}\text{Ca}_{0.2}\text{NiO}_2$ (**a**) and $\text{Nd}_{0.8}\text{Sr}_{0.2}\text{NiO}_2$ (**b**).



Extended Data Figure 4: Two-dimensional superconductivity in infinite-layer nickelates near T_c . The anisotropy ratio $\gamma = H_{c2}^{\parallel} / H_{c2}^{\perp}$ shows a diverging behaviour near T_c while approaching < 2 at low temperatures. Note that for $\text{Nd}_{0.8}\text{Sr}_{0.2}\text{NiO}_2$ at $0.73 T_c$ (see **Figure 1e**), $\gamma \sim 1.6$ is small but the $H_{c2}(\theta)$ shows a good fit to the 2D-Tinkham model. $\text{Nd}_{0.8}\text{Sr}_{0.2}\text{NiO}_2$ has a smaller γ than $\text{La}_{0.8}\text{Ca}_{0.2}\text{NiO}_2$ at all temperature range; however, its $H_{c2}(\theta)$ shows a sharper cusp near $\theta = 90^\circ$ (see **Figure 2a-b**) and suggests a more two-dimensional-like behaviour than the Ca-doped La-nickelates (see **Figure 3**) despite the smaller γ .

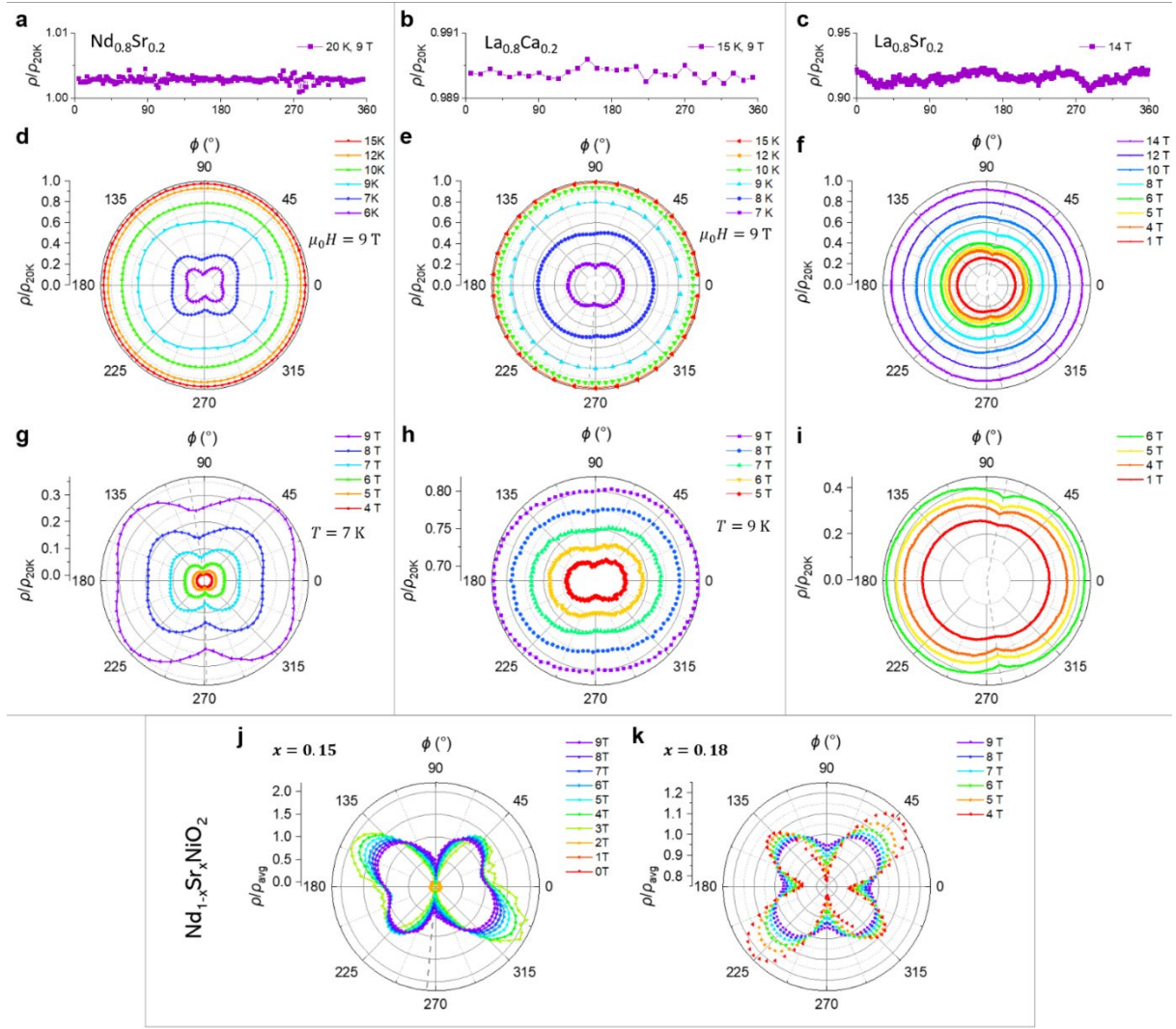


Extended Data Figure 5: Additional set of data showing the crossover from 2D-Tinkham

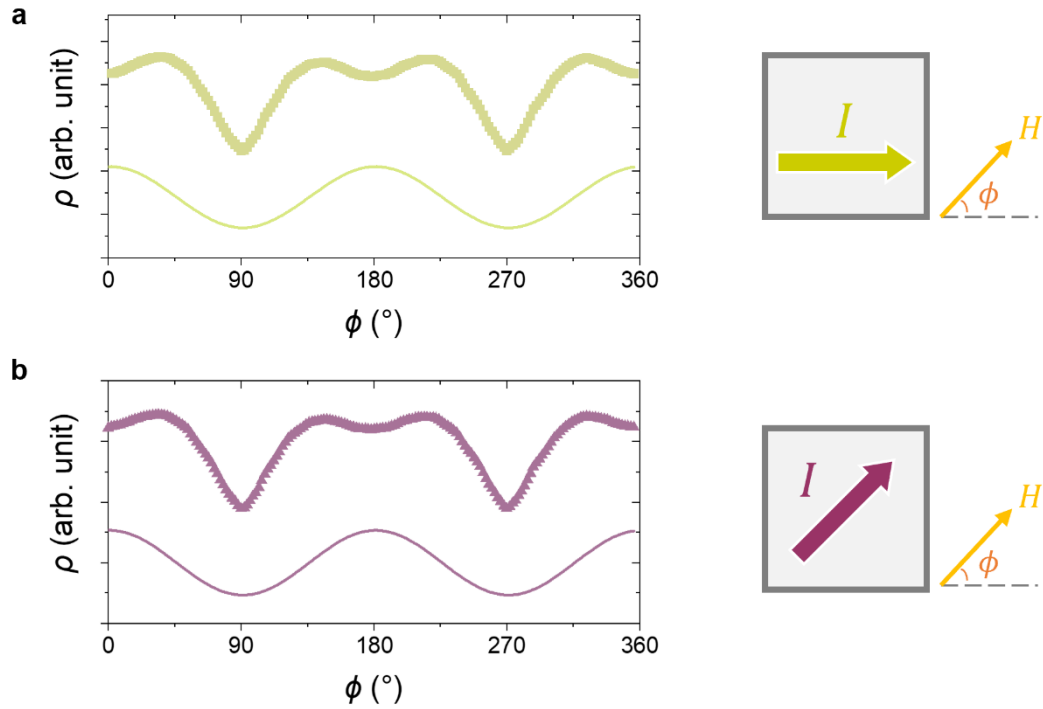
like to 3D-GL like superconducting states as $T \rightarrow 0$ K. The representative data are measured in high-magnetic pulsed-field at 0.5 K (a) and 4 K (b), respectively, on $\text{La}_{0.8}\text{Ca}_{0.2}\text{NiO}_2$ ($T_c \approx 8$ K). The

solid line 2D + 3D was fitted to the equations: $\left[\frac{H_{c2}(\theta) \sin(\theta)}{H_{c2}(90^\circ)}\right]^2 + \alpha_{3D} \left[\frac{H_{c2}(\theta) \cos(\theta)}{H_{c2}(0^\circ)}\right]^2 + \beta_{2D} \left|\frac{H_{c2}(\theta) \cos(\theta)}{H_{c2}(0^\circ)}\right| =$

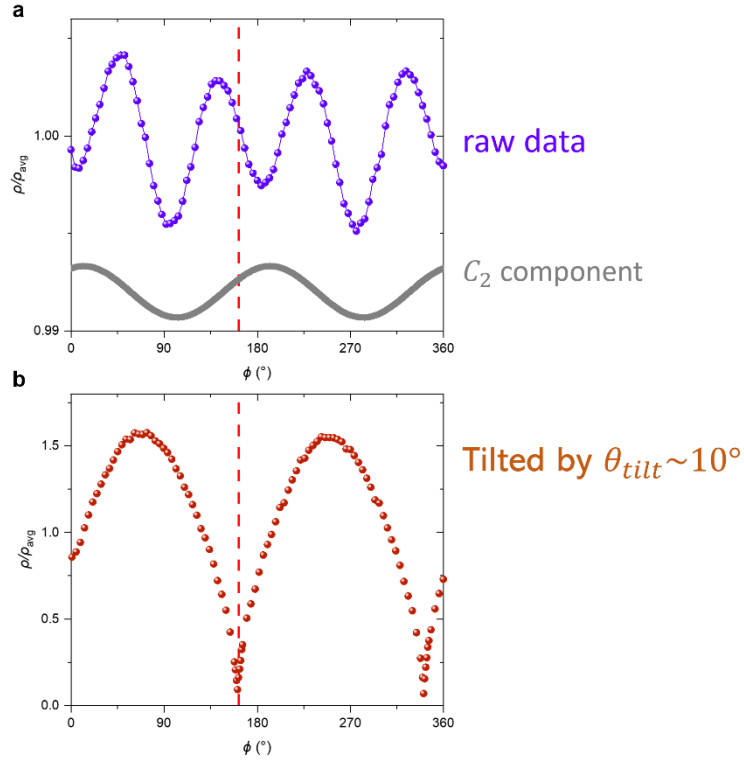
1. One can recover the 2D-Tinkham description by setting $\beta_{2D} = 1$, $\alpha_{3D} = 0$. Similarly, the 3D anisotropic mass Ginzburg–Landau model is recovered when $\alpha_{3D} = 1$, $\beta_{2D} = 0$.



Extended Data Figure 6: Anisotropic in-plane (azimuthal ϕ) angular dependent magnetoresistance $\rho[B^{\parallel}(\phi)]$ within superconducting transition. ρ_{20K} is the zero-field resistivity at 20K. ρ_{avg} is the average resistivity $\langle \rho[B^{\parallel}(\phi)] \rangle$ of various $0^{\circ} \leq \phi \leq 360^{\circ}$. (**Top a-c**) The normal state ($> T_{c,95\%}$ for **a-b**, $\sim > H_{c2}$ for **c**) shows no anisotropy in magnetoresistance as a function of in-plane field $B^{\parallel}(\phi)$. The virtually isotropic normal state $\rho[B^{\parallel}(\phi)]$ can be visualised as a circle in (**d-f**). Below T_c , a $C_2 + C_4$ symmetry can be observed in $Nd_{1-x}Sr_xNiO_2$ (**left d,g & j-k**), while only a C_2 symmetry can be observed in the La-nickelates: Ca-doped (**middle e,h**) and Sr-doped (**right f,i**). Slight asymmetric two-fold lobes (angle difference between minima are not 180° , maxima amplitude is unequal) can be observed in the La-nickelates (**i**).



Extended Data Figure 7: Anisotropic in-plane magnetoresistance when measured at two different current directions. The in-plane magnetic field $B^{\parallel} = 9$ T. Representative data was measured at 10.5 K for $\text{Nd}_{0.8}\text{Sr}_{0.2}\text{NiO}_2$ ($T_{c,95\%} \sim 16.5$ K). **(a)** current I direction points towards $\phi = 0^\circ$. **(b)** current I direction points towards $\phi = 45^\circ$. We did not observe a corresponding 45° shift in the in-plane anisotropies. The observed C_2 symmetry was not originated from the Lorentz effect.



Extended Data Figure 8: Excluding trivial origin of the anisotropic in-plane superconducting observables. The C_2 symmetric component of $\rho[B^{\parallel}(\phi)]$ are not due to trivial misalignment of field angle (with $\theta_{tilt} \neq 0$). Note that the $H_{c2}(\theta)$ fitting results show that the superconductivity has a strong 3D character at low temperature for $\text{Nd}_{1-x}\text{Sr}_x\text{NiO}_2$ and $\text{La}_{1-x}\text{Ca}_x\text{NiO}_2$, and $H_{c2}(\theta)$ shows a smooth flattened peak near the in-plane angle $H \parallel \text{NiO}_2$ plane. Therefore, the tilt effect is negligible for our study. We can further prove that this is the case by intentionally introducing a small tilt angle of $\theta_{tilt} \sim 10^\circ$ while maintaining the same in-plane orientation. Measurement on the angular dependence now shows a sharp dip (b) at a different angle $\phi_{dip} \sim 162^\circ$ from the C_2 minima in (a). The grey C_2 component curve was shifted vertically for clarity. Representative data are measured at 9 T, 11 K (a) and 3 T, 8 K (b) in $\text{Nd}_{0.8}\text{Sr}_{0.2}\text{NiO}_2$ ($T_{c,95\%} \sim 14$ K).